Journal of Physics: Conference Series **717** (2016) 012004 doi:10.1088/1742-6596/717/1/012004

Studies of high energy density physics and laboratory astrophysics driven by intense lasers

J Zhang[1,2], Y T Li[2,3], L M Chen[2,3], Q L Dong[2,4], J Y Zhong[2,5], W M Wang[2,3], Z M Sheng[1,2,6] and G Zhao[7]

[1]Key Laboratory for Laser Plasmas of Ministry of Education and Department of Physics and Astronomy, Shanghai Jiao Tong University, Shanghai, China

[2]Collaborative Innovation Centre of Inertial Fusion Science and Applications, Shanghai Jiao Tong University, Shanghai, China

[3] Beijing National Laboratory for Condensed Matter Physics, Institute of Physics, Chinese Academy of Sciences, Beijing 100190, China

[4]School of Physics and Optoelectronics, Ludong University, Yantai 264025, China

[5]Department of Astronomy, Beijing Normal University, Beijing 100875, China

[6]SUPA, Department of Physics, University of Strathclyde, Glasgow, United Kingdom

[7]Key Laboratory of Optical Astronomy, National Astronomical Observatories, Chinese Academy of Sciences, Beijing 100012, China

E-mail: jzhang1@sjtu.edu.cn

Abstract. Laser plasmas are capable of creating unique physical conditions with extreme high energy density, which are not only closely relevant to inertial fusion energy studies, but also to laboratory simulation of some astrophysical processes. In this paper, we highlight some recent progress made by our research teams. The first part is about directional hot electron beam generation and transport for fast ignition of inertial confinement fusion, as well as a new scheme of fast ignition by use of a strong external DC magnetic field. The second part concerns laboratory modeling of some astrophysical phenomena, including 1) studies of the topological structure of magnetic reconnection/annihilation that relates closely to geomagnetic substorms, loop-top X-ray source and mass ejection in solar flares, and 2) magnetic field generation and evolution in collisionless shock formation.

1. Generation and transport of laser produced hot electrons

1.1. Surface emission of fast electrons

Fast electron beams produced in ultra-intense laser-interactions with plasmas have attracted broad interest due to their potential applications in the fast ignition (FI) of inertial confinement fusion (ICF) [1], ultrafast X-ray and terahertz radiation, and so on [2]. About 20 - 50% of laser energy can be converted into hot electrons at laser intensity higher than 10^{18}Wcm^{-2}. While some of the hot electrons will be transported into overdense plasma regions, the rest of the electrons may be emitted along the target surface (or transport laterally) under certain conditions [3]. The latter can considerably enhance the hot electron density in the cone guided scheme for FI [4,5].

We have investigated the lateral transport of hot electrons comprehensively. When an intense laser pulse is incident upon a solid target with a large incident angle such as θ ~70º, as shown in figure 1(a)

a collimated hot electron beam with a divergence angle of 15°(FWHM) is emitted along the front target surface [6]. It is found that this surface electron jet is dominated for large laser incidence angles and steep electron density gradients. If there are pre-pulses with an energy of several mJ before the main laser pulse, the surface electron beam emission will be affected significantly. Another evidence for the lateral hot electron transport is obtained by K_α imaging. For θ ~70º, a horizontally asymmetric K_α halo structure has also been observed at the front surface of a Cu target, as shown in figure 1(b). The left wing of the halo extends to ~ 310 μm.

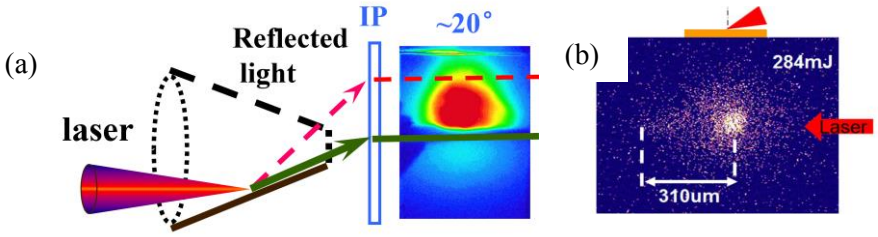

Figure 1.Measured angular distribution of > 300 keV hot electron beam (a) and K_α image (b) for θ=70°.

Hot electron beams with tight collimation, narrow energy spread and high charge are required for FI. In our recent work, highly collimated surface electron beams with MeV quasi-monoenergetic spectra are generated both in femtosecond and picosecond laser-solid interactions. In the case with fs lasers irradiating on a Cu target with a large incident angle, MeV-level monoenergetic electron beams with a divergence angle of only 1° and an average beam charge of tens of pC were obtained by optimizing the pre-pulse intensity [7]. By using the PHELIX laser in GSI and the TITAN laser at LLNL, surface electron beams with divergence angle as small as 2°, several nC charge with MeV peak energy were also generated [8].

1.2. Hot electron temperature scaling in a wide range of laser intensity

When the incident laser is at high intensity, most of the absorbed laser energy converts to the kinetic energy of hot electrons. The hot electrons follow a bi-Maxwellian distribution, i.e., $dN_e(E)/dE \sim A\exp(-E/T) + B\exp(-E/T_{hot})$, where T is the background electron temperature and T_{hot} is the hot electron temperature. Generally T_{hot} depends upon the plasma conditions (the plasma density scalelength) and the laser parameters (laser intensity, pulse duration, and laser incident angle). It scales with the laser intensity in the form of $T_{hot} \sim f(\tau, L)(I\lambda^2)^\alpha$, where $f(\tau, L)$ is a function of the laser pulse duration and the plasma density scalelength, I and λ are respectively the laser intensity and wavelength. The parameter α is a constant, which has been considered in many publications. Typically $1/4 \leq \alpha \leq 1$ under different conditions [9,10,11]. Based upon PIC simulations, we have investigated the hot electron temperature in a large range of parameters [12]. The results reveal that the value of α has a strong dependence on the dominant absorption mechanism. That is, $\alpha \sim 1/2$ when the laser intensity is high and the pondermotive acceleration dominates the absorption, which qualitatively agrees with the pondermotive potential scaling [10]. However, the value of T_{hot} can be several times higher than the ponderomotive potential, which can be attributed to the factor $f(\tau, L)$. The scaling with $\alpha \sim 1/3$ occurs at the transitional regime between resonance absorption (at lower intensities) and ponderomotive acceleration (at higher intensities).

Even though the hot electron temperatures from laser-solid interaction are confined to the scaling discussed above, there are ways to enhance the hot electron temperatures by the use of proper target designs. These introduce new absorption and/or electron acceleration mechanisms. One of the ideas is the use of a solid target with sub-wavelength structures at the front [13]. Both numerical simulations and experimental studies suggest this enhances laser energy coupling to the target, therefore both the hot electron and X-ray temperatures are enhanced [14,15]. Another idea is to adopt a target with multiple thin-slices along the laser propagation direction [16]. In this case, the inverse-free-electron acceleration mechanism works at the solid surface of the thin-slices [6,17,18], which can effectively enhance the

hot electron temperatures. The produced hot electrons are also well-collimated in the forward direction, which is beneficial both for fast ignition and laser-driven ion acceleration.

1.3. Proposal of a magnetically assisted fast ignition scheme

A key issue with the FI scheme is to enhance the heating efficiency of high intensity lasers. The first integrated FI experiment in 2001 [4] demonstrated a high energy coupling of 20%, while some subsequent experiments performed in 2008-2011 achieved a much lower coupling efficiency of only 0.7-5% [19,20,21]. Explaining the discrepancy and then further improve the efficiency is crucial for the success of FI. Integrated simulations including both generation and transport of fast electrons to simulate the plasma with densities spanning 5 orders of magnitude will be required. Recently we have realized such integrated simulations via the so-called "two-systems" PIC approach. We find that the pre-plasma formed in the cone significantly affects the coupling, which can explain the contradictory experimental observations mentioned above. To overcome such pre-plasma effect, we propose a new FI scheme [22], imposing a multi-MG magnetic field across a cone-free target, which can also avoid the asymmetry in target compression. Our integrated simulation results show that the laser-to-core coupling efficiency is enhanced 7 fold up to 14% with an external magnetic field of 20 MG, where we take two counter-propagating1 PW laser pulses of 6 ps and achieve a compressed target with a peak density of 300 g cm^{-3} and areal density of 0.49 g cm^{-2} at the core. This is attributed to the constrained fast-electron motion along the magnetic field. This simulation suggests that the magnetically assisted scheme is promising.

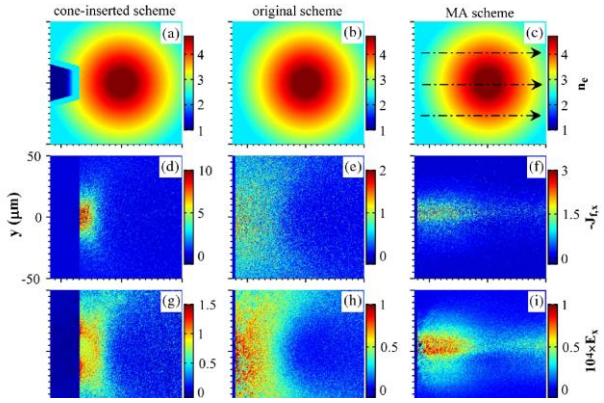

Figure 2. Snapshots of electron densities $\lg(n_e/n_c)$ initially (first row), fast-electron currents (unit of en_cc) at 2 ps (second row), and resistive electric fields (unit of $m_e\omega/c$) at 2 ps (third row). The three columns correspond to the cone-inserted, original, and magnetically assisted (MA) schemes, respectively. (f) and (i) shows that the magnetic field well confines the fast electron transport.

1.4. Controllable way for generating magnetic field larger than 100 teslas

As shown above, the magnetically assisted scheme for FI can significantly enhance the laser energy coupling to the target. Strong magnetic field of hundreds of Teslas or several MG was demonstrated on the experimental platform of ShenGuang(SG)-II laser facility by irradiating 2 kJ in 1 ns on a planar plate attached on the end of one open-ended coil [23]. The magnetic field is generated by cold background electrons to neutralize the positively charged laser foci, which has a different physical mechanism from the previous study of magnetic fields driven by hot electron current in a capacitor-coil target [24]. The strong magnetic fields generated is interesting not only for FI research, but also for other research areas including astrophysics, material science, and atomic and molecular physics, *etc.*

2. Laboratory studies of astrophysical and astronomical phenomena

Using high-power laser systems, unprecedented extreme physical conditions can be achieved at laboratories nowadays, allowing one to explore actively and controllably some important astrophysical problems. This is now called high energy density laboratory astrophysics (HEDLA) [25]. On the experimental platform of the SG II laser facility, we made some progress in HEDLA as presented below.

2.1. Modelling solar and geo-magnetic activities in laboratory

Clear evidence for magnetic reconnection in solar flares was captured [26] in X-ray and optical regions. For the slowly-developing/long-lived two-ribbon flares, a cusp-shaped bright loop formed as the reconnected separatrices are heated up by the accelerated electrons from magnetic reconnection (MR). For the short compact flare, a loop-top hard x-ray source could be produced when MR occurs above the magnetic loop as shown in figure 3(a). Solar activities also affect space environment around the Earth. Substorms of Earth's magnetosphere are produced when the solar wind arrives, compressing the geomagnetic field at magnetopause and stretching it at magnetotail. Then reconnection sites are formed locally, producing high energy particles which arrive two poles of Earth along geomagnetic field lines and excite the aurora.

Laser plasmas (LP) have strong spontaneous magnetic fields through Biermann battery effects. Therefore, experiments at the SG II laser facility can be performed by configuring a MR topology to help investigate solar eruptions and geomagnetic substorms [27,28]. In the experiments, we simply put a solid Cu target in front of the expected MR outflow. A bright spot with an area comparable to the cross section of the ion diffusion region is found when the MR outflow is ejected with enough kinetic energy. Figure 3(b) shows the comparison between the experimental result and the solar compact flare (figure 3(a)). The cartoon in figure 3(a) invokes the MR process to explain the formation of hard X-ray sources.

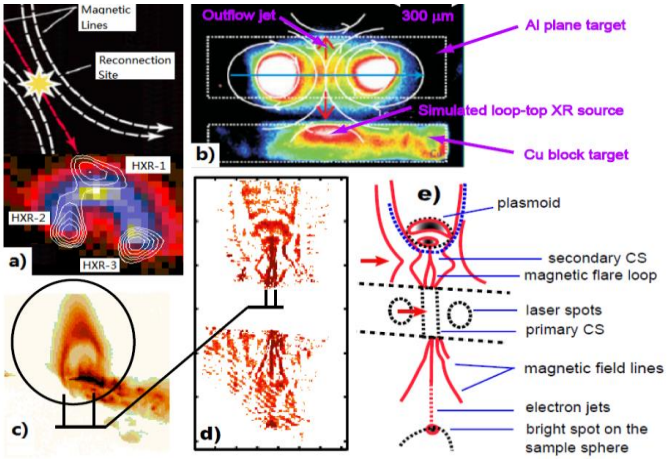

Figure 3. X-ray images of compact /short-period solar flare (a) and large/long-period solar flares (c), by Yohkoh telescope; Laser -plasma experiment results for loop-top hard x-ray emission (b); Detailed structure of MR region; (e) is the schematic cartoon of (d).

During the same series of laser plasma experiments, the moving plasmoid was also observed to stretch surrounding magnetic fields forming a flare with bright magnetic loops . Figure 3(d) gives the raw polarized image taken at 532 nm in the same series. For the clear signatures to be emphasized, a schematic picture of the experimental image is given in figure 3(e), with solid lines representing the bright lines. It is clear that the graph has two kinds of features above and below the line connecting the two laser focal spots, respectively. The upper half part of the image presents complicated features. As a whole, the fan-like region is confined by the two separatrices (or side-EDRs) as in the lower part, partially determined by the symmetrical configuration of the whole system. The detailed structure includes a bright current sheet (the 2nd CS), on the top of which exists a plasmoid with a bright spot on the bottom of it, a dark cavity, and then a bright edge located at the front. The bright spot on the bottom of the plasmoid is also connected to the 2nd CS. Attached to the other end of the 2nd CS are two bright ridges with foot-points located on the ending point of the primary/1st CS between the two mutually approaching laser-plasma bubbles, which mimics solar observations of long period flares as shown in figure 3(c). Our experimental observation confirms the theoretical prediction of possible generation of anomalous plasmoids from a current sheet. In solar CMEs, one also observed a stringy, concave-outward U-loop half-circling the ejected plasmoid from the coronal bottom. It is suspected that the U-loop in these cases might represent a detached magnetic field formed by reconnected open field lines, or some kinds of wave fronts with unclear generation mechanisms. The observation in present experiments is a plasmoid that is not yet completely detached

from the secondary current sheet within the observation duration, confirming the astronomically observed U-loop or V-loop profiles of coronal mass ejection as the reconnected magnetic field lines.

The lower part of the image presents three bright jets from the central MR site. It argues that those jets are actually three electron diffusion regions, two of which are along the separatrices. The angle between the two side-EDRs is $2\theta_{rec}\sim40^{o}$, giving the reconnection rate of 0.25-0.35. The two side-EDRs can find their counterparts in Hall-MHD simulations and astronomic observations. Mozer et al. in 2005 summarized 19 observations of EDRs along separatrices in the magnetosheath. The third/ center-EDR is rather surprising in that, besides its appearance in PIC simulations, only one event was recorded by Cluster spacecrafts monitoring the magnetotail as reported by Phan et al. in 2007, and that the astronomic observations of side-EDRs and center-EDR were made separately in different missions. In the laser-plasma experiment, however, the three EDRs were recorded in one shot. The center-EDR appeared much later than the two side-EDRs. Comparisons between astronomic observations and experimental results indicate that the lack of simultaneous observation of the three EDRs is because MR has different characteristics in different evolution stages, or the center-EDR is not within the same plane of the two side-ones, i.e., MR is truly a 3D physical process.

2.2. Laboratory study of collisionless shocks mediated by magnetic fields

Magnetic field generation, amplification and self-organization play important or even key roles in many cosmic phenomena including collisionless shocks around supernova remnants and ultrahigh energy cosmic rays that are expected to originate from the former through the so-called Fermi acceleration mechanism. For this hypothesis to be verified in laboratory, three stages of magnetic field evolution have to be confirmed, with further requirements of observations of magnetic mediated collisionless shock and its acceleration of charged particles [29].

Laser plasmas produced by high power laser pulses usually have tremendous kinetic energy. In experiments designed for the above purpose, observations of endogenous electromagnetic (EM) field transformed from kinetic energy through various instabilities within counter-streaming collisionless laser plasma is rather preferred over the Biermann magnetic field. The re-organization behaviors of the latter usually blur the identification of magnetic generation mechanisms. To realize this, two plasmas need to penetrate without collision through each other and magnetic field diagnosis should be avoided at the interface where Biermann battery effect usually dominates [30,31,32]. With such criteria, experiments were conducted in 2011 with the SG II laser facility, and the ion-plasma Weibel filamentation instability was observed with interferometry and shadowgraphy techniques [33,34]. The plasma temperature could be calculated through the measured soft x-ray emission spectra.

Figure 4(a) shows a typical shadowgraph recorded at 4.5ns after the first bunch of 4 laser beams launched to produce the left-side plasma. The filaments can be divided into two groups according to their lengths. The longer filaments of 400-600 μm are supposed to be located in or parallel to face-on planes containing two laser spots, while shorter filaments are supposed to be the projections of those filaments with larger angles to face-on planes. The dashed line gives the position where the filament distribution pattern is analyzed in figure 4(b) by using different band FFT filters. The red line presents the filtered profile involving all (short and long) filaments spaced by 90-250 μm (9.3μm/pixel), while the blue line presents only long filaments spaced by 400-600 μm as indicated by the solid triangles. Both FFT-filtered distributions reproduce the corresponding peaks /filaments in the experimental profile. It can be expected that the space among real filaments in 3D is in the range of 400-600 μm, and the smaller value of 90-250 μm is due to the "forest-effect" that the projection process usually has. Calculation of the ion-plasma Weibel instability growth rate indicated that the Weibel instability grew at $\gamma\sim4\times10^{-5}\omega_{pe}$ and $k\,c/\omega_{pe}\sim0.17$, which means, for plasmas with electron density of $5\times10^{18}cm^{-3}$, the space between filaments is around 480 μm, well in agreement with the measurements. The larger filament length in the range of 400-600 μm is another evidence for the ion-plasma Weibel instability as the inertial length is around 450 μm for the ions propagating at 500-1000km/s in plasma of 50 eV.

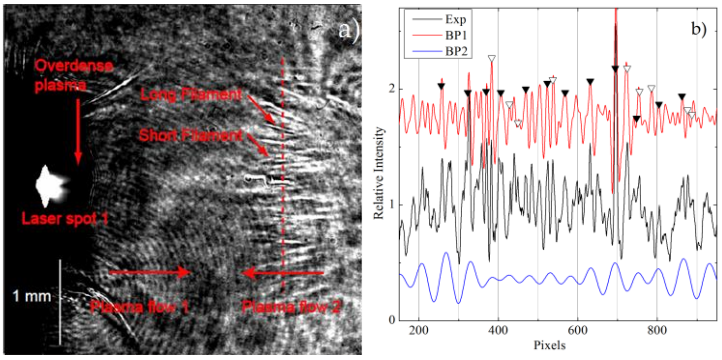

Figure 4. (a) Shadowgraph of counter-streaming plasmas, showing Weibel filamentation; (b) Filament profile analysis with BP1 for band passing of 90-250um (red line), and BP2 for 400-600um (blue line).

Acknowledgments

The authors wish to acknowledge all domestic and international colleagues contributing to the work. This work is supported by the National Basic Research Program of China (Grant Nos. 2013CBA01500), the National Nature Science Foundation of China, and Chinese Academy of Sciences.

References

[1] Tabak M *et al* 1994 *Phys. Plasmas* **1** 1626
[2] Zhang J *et al* 2005 *Appl. Phys. B* **80** 957; Zhang J *et al* 2005 *High Energy Density Physics* **1** 61
[3] Nakamura T *et al* 2004 *Phys. Rev. Lett.***93** 265002
[4] Kodama R *et al* 2001 *Nature* **412** 798
[5] Sentoku Y *et al* 2004 *Phys. Plasmas* **11** 3083
[6] Li Y T *et al* 2006 *Phys. Rev. Lett.* **96** 165003
[7] Mao J Y *et al* 2015 *Appl. Phys. Lett.***106** 131105
[8] Ma Y *et al* 2015 *Sci Sin-Phys Mech Astron* **45** 025202 (in Chinese)
[9] Sheng Z M *et al* 2015 *Chin. Phys. B* **24** 015201
[10] Wilks S C *et al* 1992 *Phys.Rev. Lett.* **69** 1383
[11] Beg F N *et al* 1997 *Phys. Plasmas* **4** 447
[12] Cui Y Q *et al* 2013 *Plasma Phys. Control. Fusion* **55** 085008 and references therein
[13] Wang W M, Sheng Z M and Zhang J 2008 *Phys. Plasmas* **15** 030702
[14] Kahaly S *et al* 2008 *Phys. Rev. Lett.* **101** 145001
[15] Mondal S *et al* 2011*Phys. Rev. B* **83** 035408
[16] Zheng J *et al* 2011 *Phys. Plasmas* **18** 113103
[17] Chen M *et al* 2006 *Opt. Exp.***14** 3093
[18] Pukhov A, Sheng Z M and Meyer-ter-Vehn J 1999 *Phys. Plasmas***6**2847
[19] Key M H *et al* 2008 *Phys. Plasmas* **15**, 022701
[20] Theobald W *et al* 2011 *Phys. Plasmas* **18**, 056305
[21] Shiraga H *et al* 2011 *Plasma Phys. Controlled Fusion* **53** 124029
[22] Wang W M *et al* 2015 *Phys. Rev. Lett.***114** 015001; *Phys. Rev. E* **91** 013101
[23] Zhu B J *et al* 2015 *Appl. Phys. Lett.* **107**, 261903
[24] Fujioka S *et al* 2013 *Rep. Sci*.**3** 1170
[25] Remington B A *et al* 2006 *Rev. Mod. Phys* **78** 755
[26] Masuda S *et al* 1994 *Nature* **371** 495; Tsuneta S *et al.* 1992 *Publ. Astron. Soc. Japan* **44** L63-L69
[27] Zhong JY *et al* 2010 *Nat. Phys.* **6** 984
[28] Dong QL *et al* 2012 *Phys. Rev. Lett.* **108** 215001
[29] Cui YQ *et al* 2015 *Sci. China-Phys. Mech. Astron.* **58** 105201
[30] Fox W *et al* 2013 *Phys. Rev. Lett.* **111** 225002
[31] Huntington C M *et al* 2015 *Nat. Phys.* **11** 173
[32] Kugland N L *et al* 2012 *Nat. Phys.* **8** 809
[33] Liu X *et al* 2011 *New J. Phys.* **13** 093001
[34] Yuan D W *et al* 2013 *High Energy Density Physics* **9** 239